Study of the L_{23} edges in the 3*d* transition metals and their oxides by electron-energy-loss spectroscopy with comparisons to theory

R. D. Leapman,* L. A. Grunes, and P. L. Fejes†
School of Applied and Engineering Physics and the Materials Science Center, Cornell University, Ithaca, New York 14853
(Received 25 November 1981)

Excitations of the 2*p* subshell in the 3*d* transition metals and their oxides have been studied by inelastic scattering of 75-keV electrons. The L_{23} "white lines" which arise from dipole transitions to unoccupied *d* states have been investigated in terms of their threshold energies, widths, and intensity ratios. Shifts in the L_3 threshold energy between the metal and oxide are different from the chemical shifts measured by x-ray photoemission spectroscopy and this suggests the importance of relaxation effects. Single-particle calculations for the L_3 spectra are also discussed. Measured L_3 linewidths are generally larger than those predicted by suitably broadened theory. A variation from the statistical L_3-to-L_2 white-line intensity ratio of 2:1 has been observed across the 3*d* transition row, with values ranging between 0.8:1 for Ti to 5:1 for FeO. This behavior appears to be associated with the white lines since Cu with a filled 3*d* band exhibits the statistical results. It is suggested that the anomalous ratios may be explained by a breakdown of *j-j* coupling caused by an exchange mechanism. Finally, the extended x-ray absorption fine-structure-type structure extending several hundred eV above the white lines is analyzed for Cr to provide the radial distribution function.

I. INTRODUCTION

The excitation of atomic inner shells by high-energy electrons or photons provides a method for studying the unoccupied conduction states in a solid. These core-level processes are mostly sensitive to final states since the initial states have narrow energy widths. Because of the predominance of dipole transitions, excitation of the 2*p* electrons for the metals of the first transition period can give information about the unoccupied 3*d* states.[1,2] Comparatively few such measurements, either by electron scattering[3–5] or x-ray absorption,[6–11] exist in the literature for this technologically important group of metals which exhibits interesting magnetic and electrical properties.

There are several reasons for the paucity of x-ray absorption (XAS) data for these L_{23} edges.[11,12] A few earlier measurements exist using conventional x-ray sources that are weak in intensity and not continuous in wavelength.[6,7] Problems associated with counting statistics and specimen-dependent nonlinearities occurred.[13] Other experiments were performed using self-absorption in x-ray emission spectra[8,9] but this method is indirect. More recently, synchrotron sources have been used to carry out x-ray absorption measurements,[11] and much accurate data has been collected at higher energies (e.g., Ref. 14). However, problems have been encountered in the energy range 400–1000 eV, where the L_{23} edges in the 3*d* transition metals lie. This has been largely due to damage and contamination of the crystals required to monochromatize the intense photon flux from the synchrotron.[12] As is now well established fast electron scattering provides an alternative method for exciting core levels (e.g., Refs. 3–5, 15 and 16). Although much data has been obtained in the range of energy losses below 300 eV, few instruments have been able to provide well-resolved data at higher energies.

The purpose of this paper is to present a systematic study of core excitation spectra for metals in the 3*d* transition row and their oxides. We (R.D.L. and L.A.G.) have recorded electron-energy-loss spectra (EELS) at 75-keV incident energy from thin films in a transmission electron microscope combined with a Wien filter spectrometer capable of 1-eV resolution.[17] This system has an important advantage of allowing the accurate characterization of the sample in terms of a selected area electron diffraction pattern and an image, while spectra can be obtained from precisely the same region. We shall examine our data to establish trends within the period and to compare results with theory.

Previous work has shown that the 3d transition metals have L_{23}-edge spectra dominated by intense sharp peaks a few eV wide.[3–11] These are also seen in the L_{23} edges of the other transition periods and have been dubbed "white lines" since they were first discovered in x-ray absorption spectra recorded on photographic film.[2] The white lines result from transitions from the 2p levels to the large unoccupied 3d density of states. We observe variations in the relative intensities, widths, and energies of these white lines, between different metals and between a metal and its oxide.

In the case of x-ray absorption, dipole selection rules apply ($\Delta l = \pm 1$) so the final states have s or d symmetry, the d states being by far the most strongly peaked and the most favored in the transition.[18] The photoabsorption cross section is thus written within the single-electron model and the first Born approximation in terms of a dipole matrix element between an initial core state $\langle i \mid$ and final state $\mid f \rangle$ as[18]

$$\sigma_{\rm abs}(E) = \frac{4\pi^2 e^2}{\hbar c} E \mid \langle f \mid \hat{e}\cdot\vec{r} \mid i \rangle \mid^2 , \tag{1}$$

where E is the photon energy and $\hat{e}$ is a unit vector in the direction of the electric field. The cross section for inelastic scattering in a transition between two similar states is given by[19]

$$\frac{d^2\sigma(E,q)}{dE\,dq} = \frac{8\pi e^4}{\hbar^2 v^2}\frac{1}{q^3} \mid \langle f \mid \exp(i\vec{q}\cdot\vec{r}) \mid i \rangle \mid^2 , \tag{2}$$

where $\vec{q}$ is the momentum transfer, E is the energy transfer, and v is the incident electron velocity. Equation (2) can be expanded as

$$\frac{d^2\sigma(E,q)}{dE\,dq} = \frac{8\pi e^4}{\hbar^2 v^2}\frac{1}{q^3}\left|\left\langle f\left|1+iq(\hat{\epsilon}_q\cdot\vec{r})-\frac{q^2}{2}(\hat{\epsilon}_q\cdot\vec{r})^2+\cdots\right|i\right\rangle\right|^2 , \tag{3}$$

where $\hat{\epsilon}_q$, a unit vector in the direction of $\vec{q}$, plays the role of the electric field polarization vector $\hat{e}$ in the case of x-ray absorption. Within the small-scattering-angle approximation, which requires the momentum transfer $q \ll r_c^{-1}$ where r_c is the radius of the core orbital, the matrix element in Eq. (3) can be reduced to $\langle f \mid \hat{\epsilon}_q\cdot\vec{r} \mid i \rangle$, and the quadrupole and higher-order terms can be neglected.[20] The differential cross section is then of the same form as that in Eq. (1), so in this limit we expect a complete correspondence between energy loss and photoabsorption data, as is well known (e.g., Ref. 21).

While in the 4d and 5d transition elements the L_3 and L_2 edges ($2p_{3/2}$ and $2p_{1/2}$ excitations, respectively) are well separated in energy, in the 3d transition elements the spin-orbit splitting is only 5–20 eV, so structure from the two edges overlaps. The factors which govern the relative strengths and shapes of these white lines are not completely understood, and this work sets out to investigate them experimentally. We also compare our data with previous L_{23} edge measurements. In addition to XAS and other EELS data we consider x-ray photoelectron spectroscopy (XPS). The latter probes the occupied core levels and is less sensitive to the state of the excited electron, provided the incident energy is much greater than the core-binding energy. Such data are useful in determining the binding energy of core levels with respect to the highest occupied valence states in the sample.[22]

In the single-particle approximation, the measured intensity in the energy-loss (or photoabsorption) spectrum above an inner-shell edge may be decomposed into the product of an energy-dependent matrix-element factor $P(E)$ and a projected density of states $N(E)$ with appropriate symmetry[2]:

$$I(E) \propto P(E)N(E) . \tag{4}$$

The fine structure near the core-edge onset is therefore expected to reflect the density of states obtained from a band-structure calculation only if the matrix-element factor is slowly varying in that energy region. With the advent of new computing techniques and larger, faster machines, theoretical one-electron band calculations extending several rydbergs above the Fermi level have recently become possible.[23,24] We compare our measured results with calculations for the absorption spectra. While we find that the general features of our spectra for the metals can be understood in terms of state densities, striking variations in the relative white-line intensities are as yet unexplained.[5] Further, no theoretical calculations exist with which to compare the observed spectral changes upon oxidation.

II. EXPERIMENTAL

A. Instrumentation

The experimental system for recording the spectra has been described previously.[17] This consists

of an HU11A transmission electron microscope combined with a retarding field Wien filter spectrometer. Using the electron microscope in the selected area diffraction mode, a 4-μm spot of 75-keV electrons is incident on the specimen with a beam divergence of less than 10^{-3} rad. An entrance slit to Wien filter spectrometer selects electrons according to their scattering angle and the spectrometer disperses them in a direction perpendicular to the slit. Spectra are recorded by scanning the energy-loss intensity across an aperture and scintillator and counting single pulses from a photomultiplier. In the present experiments the aperture subtended a scattering angle of ± 2 mrad corresponding to momentum transfers up to 0.3 Å^{-1} for which the dipole approximation (above) holds. In order to extend the energy range of the spectrometer to the core-edge region of several hundred eV, a -3-kV adjustable power supply has been installed (P.L.F.). The ground of this supply is connected to the electron-gun high voltage, enabling the spectrometer offset voltage to float. Thus the spectrometer setting is insensitive to fluctuations in the microscope high voltage. The power supply provides a manually adjusted energy-loss offset, while digital scans of an additional 0—200 eV are controlled by a microcomputer, which also stores and displays the spectrum.[25,26] After acquisition, the data is uploaded to a PDP11/20 computer for processing. Since the spectrometer has a resolution of better than 0.1 eV, the energy resolution of the measured spectra (1 or 2 eV) is determined mainly by the thermal spread of the incident beam. Absolute measurement of the energy losses is accurate to about 0.5 eV.

B. Samples

Thin polycrystalline metallic films were prepared by electron-beam evaporation in an ion-pumped high-vacuum system at a base pressure of about 2×10^{-8} Torr. Film thicknesses of 15-nm titanium, 15-nm chromium, 26-nm iron, 9-nm nickel, and 24-nm copper were measured using a quartz-crystal thickness monitor situated near the substrate, which was the (100) face of a cleaved rock-salt crystal. All the metal films obtained in this way were polycrystalline with a grain size between 5 and 100 nm. They were floated off in ethanol and supported on 3-mm diam. copper grids (400 mesh per inch). Oxide films were prepared by heating in air metal films already supported on grids. The samples were all characterized by means of electron diffraction and imaging in the microscope before data collection. The polycrystalline ring diffraction patterns were matched to the d spacings as given by the x-ray powder diffraction file.[27] This enabled us to determine the oxidation state of the oxide films and also to verify the metal film purity. Grain sizes for the oxides were generally larger than those for the metals, resulting in sharper rings. Images and indexed diffraction patterns are shown in Figs. 1(a) and 1(b) for Ni, and in Figs. 1(c) and 1(d) for NiO. In the case of Ti a 4-nm Cr film was evaporated on both sides to protect the metal against oxidation. It is noted that absorption of Cr into Ti is less than 1% (Ref. 28), and the Cr and Ti L_{23} edges were sufficiently separated to eliminate peak overlap problems. There was little sign of an oxygen K edge in the metal energy loss spectrum (see below), indicating that the films were reasonably pure.

One of the most important considerations in our experiment besides specimen composition is specimen thickness. Because electrons interact strongly with matter, the probability of plural scattering involving valence-electron excitation is large for thick films.[29] The effect of plural scattering on the core edges is to convolute the desired single-

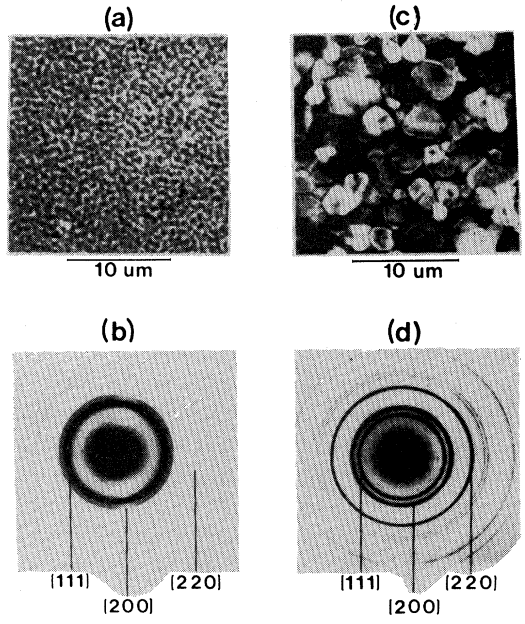

FIG. 1. (a) Electron micrograph of Ni foil showing a grain size of $\sim$20 to 40 nm. (b) Electron diffraction pattern of fcc Ni foil. (c) Electron micrograph of NiO foil showing a grain size of $\sim$2 to 4 μm. (d) Electron diffraction pattern of fcc NiO foil.

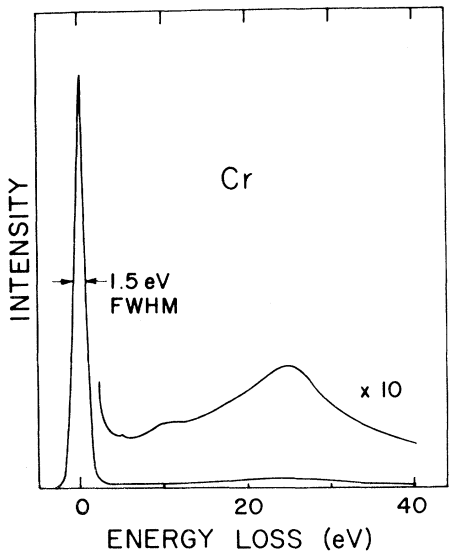

FIG. 2. Energy-loss spectrum from 15-nm Cr foil up to energy loss of 40 eV. A broad plasmon peak is seen at 22.5 eV.

scattering distribution by the low-loss region of the spectrum. This produces additional peaks at the plasmon energies (<25 eV) above edge onset and otherwise distorts the spectrum. The total mean free path for inelastic scattering is typically 50 nm, at the incident beam energy of 75 keV used in our experiment. A sample thickness $\ll 50$ nm should therefore be chosen to minimize these effects and this has been done in the present work. An estimate for the amount of plural scattering can be made by measuring the intensity ratio of the plasmon- and zero-loss peaks. To illustrate this we show in Fig. 2 the energy-loss spectrum integrated over all scattering angles for Cr up to 40 eV. Even though plural scattering is discernible its effect on the core edge within the first 20 eV above threshold is small and can be neglected for analysis of the near-edge fine structure.

Thickness effects are also important in x-ray absorption measurements[13] with which we shall compare our data. These come about because of the finite resolving power of x-ray spectrometers (energy width of the monochromated beams) and also from the presence of impurity wavelengths. In the region close to threshold where sharp lines occur, the measured absorption coefficient can be strongly thickness dependent (e.g., Refs. 2 and 6). Also, irregularities in thickness over the $1-10$ mm^2 sample area being probed can lead to further spectral distortions. For the 3d transition-metal L spectra, the optimum thickness of 1/(x-ray absorption coefficient) is only about 0.3 μm, and it is difficult to produce a large uniform foil so thin. It is not clear to what extent nonlinearities are present in synchrotron x-ray absorption spectra recorded by electron yield, which is essentially a surface technique.[12] Although corrections can be applied for some of these effects,[30] it is difficult to eliminate them completely. Consequently, the relative peak intensities of existing x-ray absorption data are probably less reliable than those of the equivalent electron-energy-loss data, although the peak energies may be measured accurately by both methods.

III. RESULTS AND DISCUSSION

A. General features of the 2p core edges

Before examining in greater detail the shapes of the 2p edges at a resolution of ~ 1 eV we first present in Figs. 3—6 spectra recorded with ~ 2 eV resolution over an extended energy range for Ti, Cr, Ni, and Cu together with their oxides. These

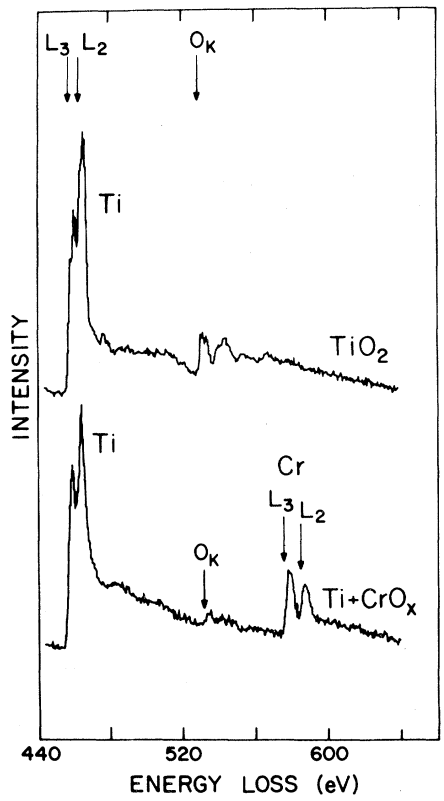

FIG. 3. L_{23} edge in Ti and TiO_2 over an extended energy range. In the metal the Cr L_{23} edge is also visible due to a protective layer of Cr coating the Ti. In TiO_2 spectrum. The oxygen K edge is seen at 531 eV.

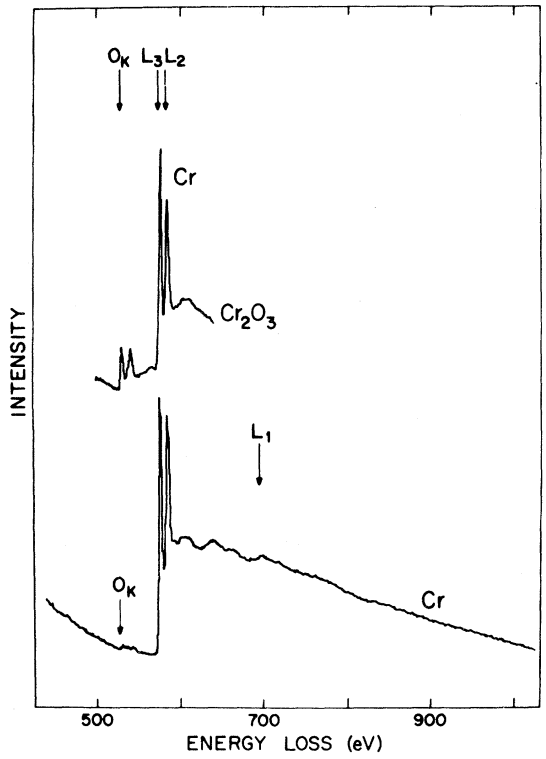

FIG. 4. L_{23} edge in Cr and Cr_2O_3. The Cr spectrum extends over 400 eV above threshold and includes the L_1 edge at 696 eV. The oxide spectrum shows a strong O K edge at 531 eV.

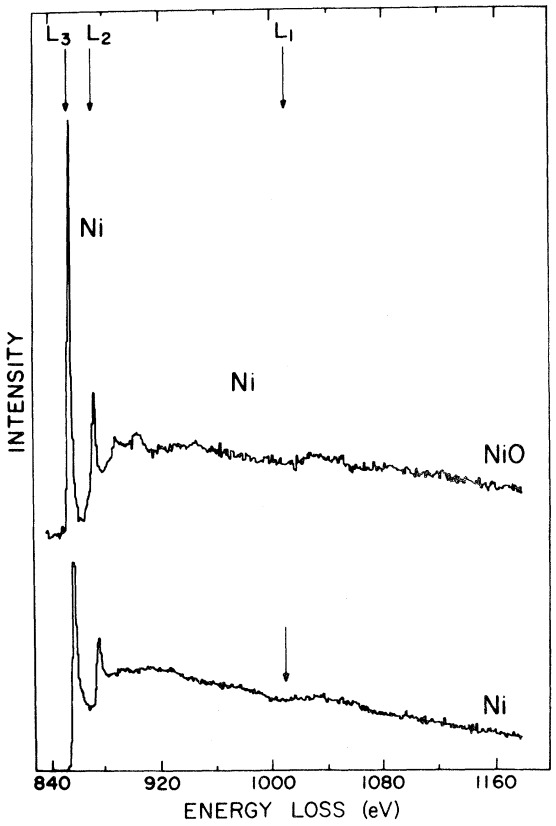

FIG. 5. L-edge spectra over an extended energy range for Ni and NiO, showing strong L_{23} white lines.

figures show the relative magnitude of different features in the spectra. The sharp double peaks at threshold arise through transitions from the $2p$ core levels to the narrow unoccupied d states in the transition elements. Lowest in energy is the transition from the $2p_{3/2}$ level (L_3 edge) which is separated from the $2p_{1/2}$ transition (L_2 edge) by the spin-orbit splitting. This energy difference increases across the period from 6 eV in Ti to 20 eV in Cu, in agreement with binding energy data.[31] Copper metal has a filled $3d$ band and hence does not exhibit sharp white lines; only steps are seen at the two edges.

In the case of Ti and TiO_2 (Fig. 3), the L_{23} white lines overlap, but are clearly resolved. The Cr L_{23} peaks appearing in the Ti spectrum at 575 and 585 eV are due to excitations from the 4-nm chromium oxide thicknesses sandwiching the Ti film and acting as an oxide barrier. The success of this scheme is evaluated by comparing the integrated area under the oxygen K edge (531 eV) in TiO_2 with that of the residual oxygen peak in the chromium coated Ti, yielding an upper limit of $\sim 10\%$ oxidation. Further, the onset energy of the residual oxygen K edge corresponds to that of oxy-

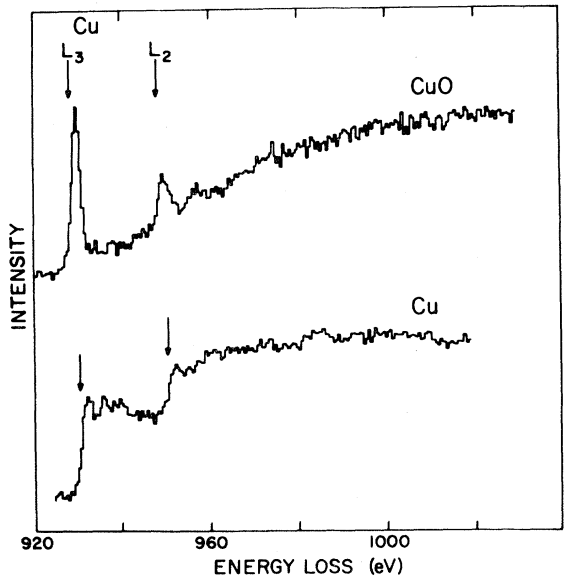

FIG. 6. L_{23} edge spectra from Cu and CuO extending ~ 100 eV above threshold.

gen embedded in chromium rather than in Ti.[32] The L_{23} white lines in the 3d transition metals are all highly visible above the pre-edge background. In the case of Ti, we measure a jump ratio of 2.7:1 for the first peak. Intensity modulations after the L_{23} lines are equivalent to extended x-ray absorption fine structure (EXAFS), and this complicates the spectral shape in the region of the oxygen K edge in TiO_2. EXAFS analysis has been carried out by Denley *et al.*[11] for the titanium L_{23} edge in recent synchrotron x-ray absorption measurements recorded at an energy resolution of ~ 5 eV. Such a resolution just resolves the two white lines but is quite adequate for determining the radial distributions from the slowly varying EXAFS modulations.

In chromium the spin-orbit splitting has increased to 9 eV and the white lines are better separated, as seen in Fig. 4. The EXAFS modulations in Cr metal are easily visible and we show below how this data can be tranformed to give the radial distribution function. A proper analysis requires that we take into consideration the L_1 edge (2s shell) which is comparable in amplitude to the EXAFS modulations. This 2s excitation to states of p symmetry appears as a weak edge at 696 eV in Fig. 4. The unoccupied p states are much more spread out in energy than the sharply peaked d states, and hence we do not expect a narrow white line at the L_1 threshold. Since the 2s level has a shorter lifetime than the 2p level, it has a greater energy width associated with it[33,34] (~ 5 eV for the L_1 shell compared with ~ 0.3 eV for the L_3 shell). This causes a further broadening of the L_1 edge. We note the virtual absence of an oxygen K edge in the Cr spectrum, assuring us of the relative purity of the metal, while Cr_2O_3 exhibits a prominent oxygen K edge, as well as the sharp L_{23} peaks.

Spectra for Ni and NiO in Fig. 5 are again dominated by strong white lines. In the ensuring figures, we have stripped off the pre-edge background by fitting it to a power law of the form AE^{-r}.[35] In Fig. 5, the intensities far above threshold (at 1000 eV) were normalized to the same value for both spectra. After normalization it is apparent that the white-line intensity relative to the slowly decreasing tail increases dramatically in the oxide with respect to the metal. Also we see that the intensity after the L_3 peak falls almost to the background level. EXAFS modulations and a weak broad L_1 edge (1008 eV) are evident in both metal and oxide. Kiyono *et al.*[10] have measured the Ni L_{23} edge up to 1300 eV by x-ray absorption using a conventional x-ray tube source and we find our data to be in good agreement.

In the case of copper and copper oxide the background was subtracted and the intensities normalized to the same value at ~ 1000 eV as was done for nickel. Figure 6 shows that the resulting spectra have poorer counting statistics than for the lower Z elements as expected from the decreasing cross section with increasing energy loss. (In an attempt to maximize signal, we have increased the filament current and the resulting energy resolution has been degraded to ~ 4 eV.) The absence of a white line for copper is due to a filled 3d band. Only steps are present corresponding mainly to transitions to the relatively flat region of the density of states with some d character. Transitions to s states, although allowed by the dipole selection rules, are much less important.[18,24] The reappearance of white lines in CuO suggests a partial emptying of the Cu 3d band. However, their relative intensity is much reduced in relation to the transition-metal oxides above. Our measured spectrum for copper is consistent with the x-ray absorption data of Bonnelle[6] and Kiyono *et al.*,[10] which also

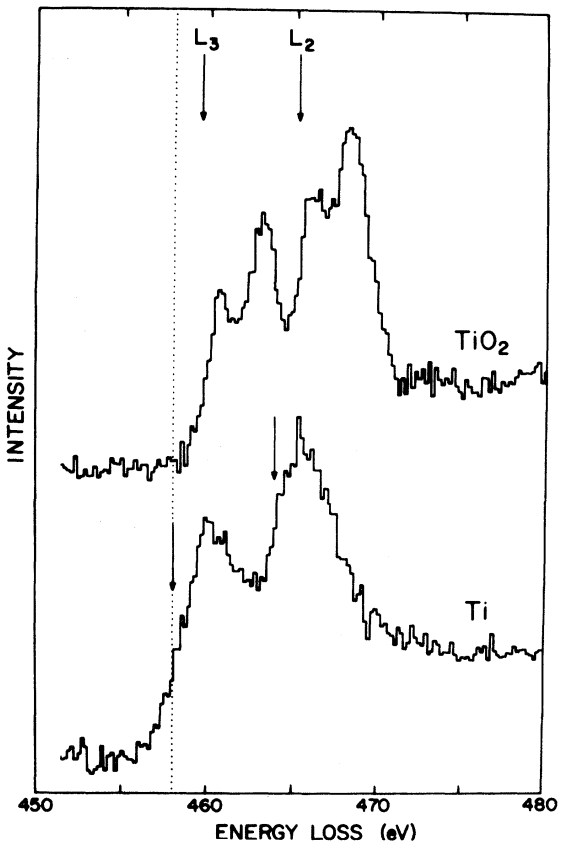

FIG. 7. L_{23} white lines in Ti and TiO_2.

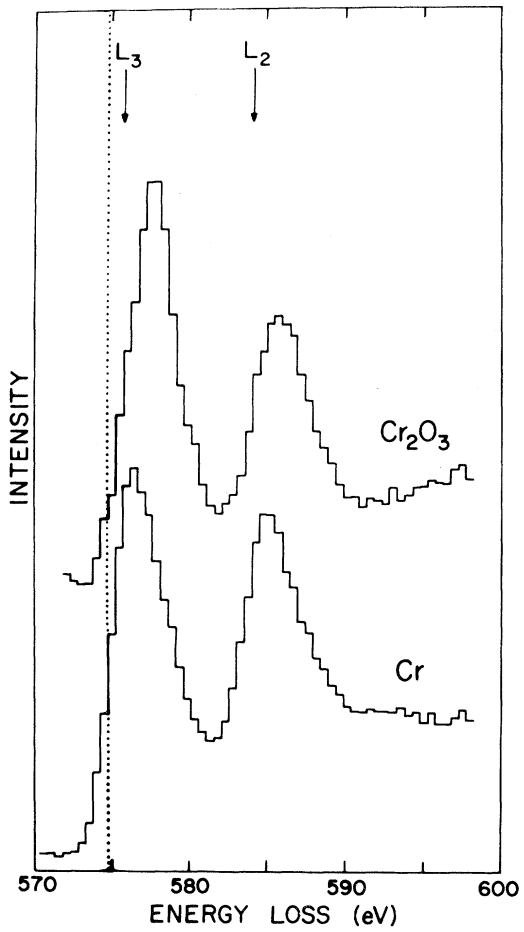

FIG. 8. L_{23} white lines in Cr and Cr_2O_3.

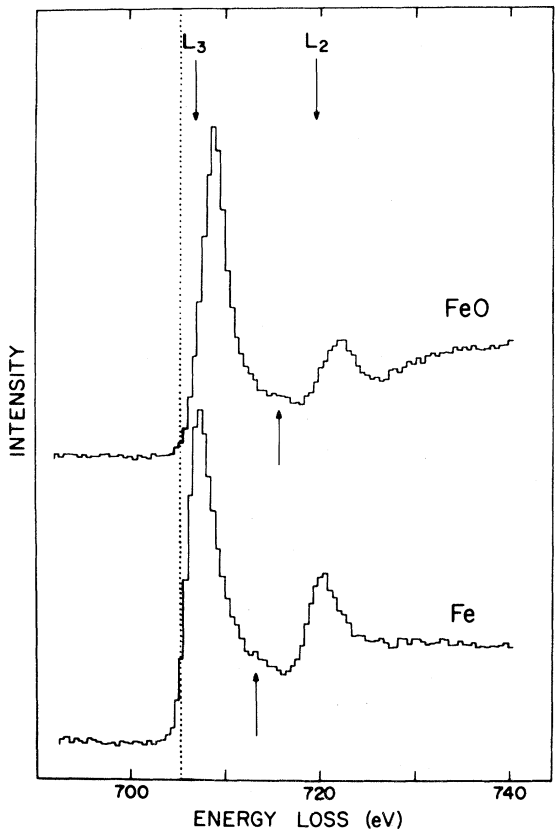

FIG. 9. L_{23} white lines in Fe and FeO.

show no white lines at threshold. The fine structure visible near the L_{23} edges in Fig. 6 is discussed below.

B. Chemical shifts and fine structure

We now examine with a higher energy resolution of ~ 1 eV the spectral shapes in the vicinity of the L_{23} white lines. We consider first shifts in threshold energy and later variations in fine structure between a metal and its oxide. Results for Ti, Cr, Fe, Ni, and Cu together with their oxides are shown in Figs. 7–11, respectively. In all cases the background intensities preceding the edge have again been fitted to an inverse power law and subtracted off so that only the L_{23} intensity remains.[35] Multiple scattering by a core loss and a bulk plasmon which would occur at ~ 20 eV above the L_3 (L_2) threshold is plainly absent from the Ti, Cr, Fe, and Ni spectra. For Cu a plasmon superimposed above the L_3 white line would coincide with the L_2 onset, but from the rest of the spectra we may safely infer that multiple scattering is unimportant. Hence the measured intensities are essentially the single-scattering distribution.

Our measured EELS L_3 edge energies are listed in Table I. We note that although the absolute value of the threshold energy measured from the half-height of the white line was only accurate to ± 1 eV, the shift of the L_3 edge in the metal relative to the oxide could be measured to within ± 0.2 eV. This accuracy was achieved by mounting both the metal and oxide films on the same grid so that spectra from both could be recorded in rapid succession in the electron microscope with the spectrometer offset fixed.

For purposes of comparison, we also list in Table I x-ray photoemission spectroscopy (XPS) L_3 metal binding energies,[31] and also the reported XPS "chemical shifts"[36–40] between metal and oxide energies at onset.[41] (In XPS, a high-energy photon is absorbed, exciting the core photoelectron to states far above the Fermi level. The photoelec-

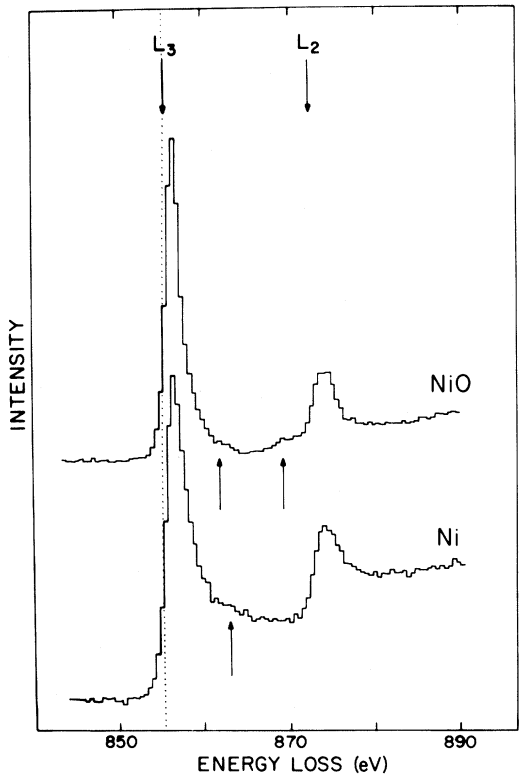

FIG. 10. L_{23} white lines in Ni and NiO.

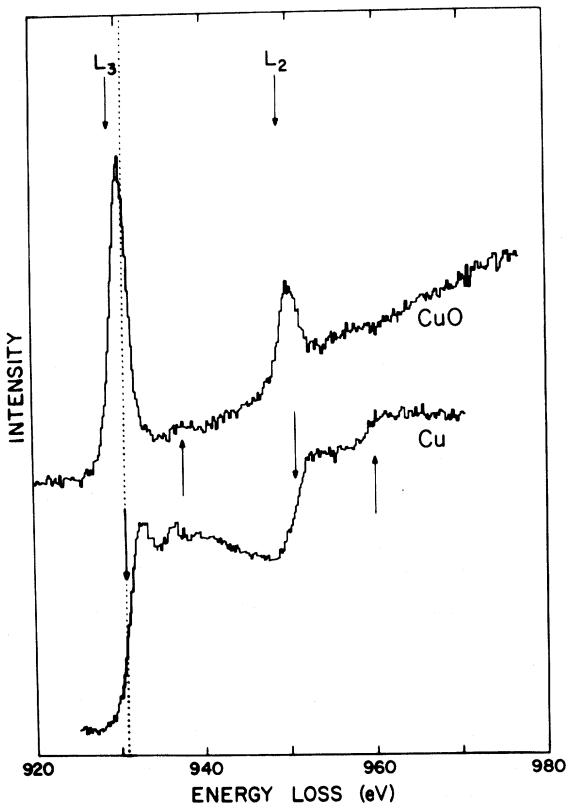

FIG. 11. L_{23} edges in Cu and CuO.

tron then exits the target where it is detected using an energy dispersive analyzer.) We see from Table I that for the metals, the XPS binding energies are generally in good agreement with the EELS edge energies. However, the two sets of chemical shifts differ markedly. In particular, the XPS differences (oxide-metal) are significantly larger than our EELS differences. Further, in photoemission, the oxide L_3 binding energy is always larger than in the corresponding metal, whereas in energy loss, the oxide-edge energy is found to be sometimes higher (Ti,Cr,Fe), sometimes lower (Ni,Cu) than in the metal.

In an attempt to interpret these observations, we resort first to a simple one-electron transition scheme shown diagrammatically in Fig. 12. In

TABLE I. L_3-edge energies determined from the EELS spectra for the oxides and the corresponding metals. The L_3 binding energy of the metals determined from XPS (Ref. 31) is also shown and the XPS chemical shift between the metal and oxide L_3 energy is compared with the EELS chemical shift. The difference between the two appears in the next column, and is larger than half the oxide band gap.

Oxide	EELS L_3 edge energy Oxide	Metal	EELS chemical shift of L_3 edge (oxide-metal)	XPS L_3 metal binding energy	XPS chemical shift of L_3 edge (oxide-metal)	Ref.	Difference in chemical shifts (XPS−EELS)	Oxide band gap	Ref.
TiO_2	459±1	458±0.2	1.4±0.2	455±1	4.9±0.3	36	3.5±0.5	3.0−3.9	48,49
Cr_2O_3	576	575	1.0	576	2.6	37	1.6	1.6−2.1	49,50
FeO	707	706	1.4	707	3.8	38	2.4	3.7	51
NiO	854	854	−0.2	854	1.6	39	1.8	3.7	49,51
CuO	931	933	−2.1	933	1.1	40	3.2	2.0	52

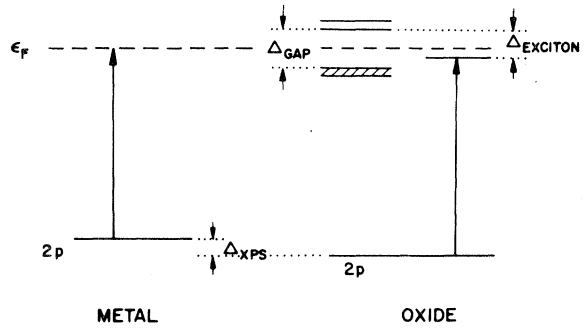

FIG. 12. Energy-level diagram showing initially proposed relation between XPS chemical shift, Δ_{XPS}, and the difference in EELS threshold energies between the metal and oxide. This depends on the band gap, Δ_{gap}, and the core exciton shift, Δ_{exc}.

both the XPS and EELS experiment, an electron is ejected from the $2p$ core level. In XPS the excited electron has a large kinetic energy of, typically, a few hundred eV or more. Hence the final state of the XPS core electron is essentially independent of the sample band structure and we expect the metal-oxide chemical shift to be a measure of the difference in energy between the respective $2p$ core levels. The difference is labeled "Δ_{XPS}" in Fig. 12, where the oxide $2p$ level is shown as lying deeper than in the metal. (Upon oxidation, valence-electron charge is transferred from metal to oxide, altering the atomic potential. Shielding of the $2p$ orbitals is slightly diminished resulting in an increase in the oxide core-level energy.[42])

In EELS or XAS, a core hole is also created via excitation of the $2p$ electron. However, in contrast to XPS, at threshold this electron is excited to the lowest unoccupied states in the material. Hence the measured edge energy depends strongly on the band structure. For a metal, the transitions at threshold are to the unfilled portion of the conduction band lying just above the Fermi level (Fig. 12). The oxides considered herein are all insulators. Hence a band gap "Δ_{gap}" appears between the filled valence and unfilled conduction bands, with the Fermi level, ϵ_F, near the center. Also in insulators, the core hole is incompletely screened from the excited electron and a core exciton final state may be formed,[22,43–47] lowering the excitation energy by "$\Delta_{exciton}$." The resulting transition is shown in the oxide portion of Fig. 12. From this figure, we now deduce the relationship between the metal-oxide core-level chemical shift is measured by EELS vs XPS:

$$\Delta_{XPS}-\Delta_{EELS}=\Delta_{exc}-\Delta_{gap}/2\ . \qquad (5)$$

The difference between the XPS and EELS chemical shifts along with the reported oxide band gap[48–52] are listed in Table I. Using these numbers in Eq. (5), we find a disconcerting result, namely, that the excitonic shift is usually found to be greater than the band gap between the valence and conduction bands. This implies that the core exciton state lies at an energy below the top of the valence band, a highly unphysical result.[53] This finding signals a breakdown of our single-electron transition scheme for interpreting these chemical shifts.

In order to find an explanation for this apparent discrepancy in the interpretation of our chemical shift data, we must take into account various many-body relaxation effects which alter the above single-electron transition picture. Quantitative treatment of such effects has not been attempted for the materials under study and is beyond the scope of this paper. We present here only a qualitative discussion in order to suggest an explanation for the inadequacy of the above approach.

When a core electron is ejected in either EELS or XPS, a hole of positive charge is created toward which the remaining one-electron orbitals relax adiabatically. In XPS, additional energy is imparted to the outgoing electron, reducing the core-level binding energy by ϵ_r, the relaxation energy.[54] In EELS, the energy transfer from the incident high-energy electron to the excited core electron is reduced by ϵ_r. In either case, then, relaxation lowers the measured energy of onset from the original one-electron orbital value. This effect is greater in metals, where the valence charge is more effective at screening, than in insulators, where screening is less.

Herbst and Wilkins[55] have undertaken systematic calculations for the excitation energies of the $3d$ levels in rare-earth metals. In order to obtain agreement with the experimental XPS binding energies, they find it necessary to include the effects of the fully relaxed core hole. For the M_{45} level of La at 844 eV, an energy similar to the L_{23} levels studied in the present work, the relaxation correction amounts to 20 eV. Calculations for the $2p$ relaxation energy in atomic Mn and Cu are of similar magnitude.[56] Hence relaxation is a significant effect, and small differences in it between the different core spectroscopy processes could easily be of the same magnitude as the differences in the measured chemical shifts.

Indeed, one might well expect relaxation in XPS vs EELS to be inequivalent since the perturbations to the electronic system produced by these two ex-

periments *are quite distinct.* In EELS (and in x-ray absorption as well) the excited 2p electron is promoted to a localized 3d state. Therefore, the core hole remains screened and the distribution of valence electrons is similar to the ground state. In XPS, on the other hand, the excited electron is ejected to energies far above the Fermi level, leaving behind the bare core hole. As noted previously, the reaction to the core hole is quite different in the metal and in the oxide. In the metal, the core hole is well screened by a relaxation of the other conduction electrons, while in the oxide, which is an insulator, the core hole is poorly screened. These differences in screening and relaxation between XPS and EELS and further between a metal and its oxide probably lead to the difference in chemical shifts observed between the two experiments.

In addition to differences in threshold energy, we also observe fine-structure variations between the metal and oxide spectra shown in Figs. 7—11. We consider first the spectra of Ti and TiO_2 shown in Fig. 7. Despite the similar shapes of these spectra over a broad energy range (Fig. 3) we now see that each of the L_3 and L_2 peaks in the oxide is split into two components separated by 2.5 eV. The L_3-L_2 spin-orbit splitting of 5.5 eV in both Ti metal and TiO_2 agrees closely with the XPS binding energy data of Cardona and Ley[31] who give a value of 6.1 eV. Our spectrum for Ti metal is consistent with a previous energy loss measurement by Trebbia[4] recorded at $\sim$3 eV resolution. The only data for TiO_2 are x-ray self-absorption measurements by Fischer *et al.*[8,58] extending to the L_2 edge onset. In these spectra the L_3 peak is also seen to be split into two components and this is explained in terms of the crystal field. Fischer's interpretation[8] of the spectrum uses the cluster molecular-orbital approach rather than the density of states derived from band structure; octahedral coordination of Ti atoms with oxygen splits the degenerate unoccupied 3d states into a lower energy $2t_{2g}$ molecular orbital level and a higher energy $3e_g$ level. Such a molecular orbital description may be reasonable for the transition-metal oxides where states are expected to be localized, but it can only predict spectral peak energies, not their shapes or widths. For the metals a band-structure model is necessary, and this is also desirable for the oxides.

For the case of Cr and Cr_2O_3 no additional fine structure is resolved in the vicinity of the L_{23} white lines. Figure 8 shows that whereas the L_3 and L_2 lines are asymmetrical in the metal, rising more abruptly on the low-energy side, in Cr_2O_3 they are nearly symmetrical. This shape, which we find in TiO_2 as well as the other oxides, is further evidence for excitonic behavior as discussed by Brown *et al.*[59] The skewed shape seen in the metals indicates a high density of states embedded in a continuum.[2]

We can compare our EELS Cr and Cr_2O_3 measurements with x-ray self-absorption data of Fischer[9] who finds additional weak structure within the L_3 and L_2 peaks having 1 eV or so spacings. The general shape of Fischer's spectrum fits with ours and also with other x-ray absorption work on Cr metal by Bonnelle[6] and Brytov *et al.*[7]

A difference in line shape between metal and oxide is also evident for Fe and FeO in Fig. 9. The Fe L_3 and L_2 edges are separated by a spin-orbit splitting of 13 eV and the two edges have similar shapes. Between the two white lines there is a subsidiary weak shoulder in the Fe spectrum at 714 eV and also a weak shoulder in FeO at 716 eV. The metal spectrum is consistent with the x-ray absorption data of Bonnelle[6] who finds a similar feature above the L_3 edge.

In Ni and NiO, the existence of a core exciton is again supported by the symmetrical L_3 line shape in the oxide compared with the skewed shape in the metal. A weak shoulder is observed in the Ni spectrum between the L_3 and L_2 edges at 862 eV, again in agreement with Bonnelle's data.[6] The NiO spectrum has a weak shoulder at 861 eV and the intensity falls almost to zero, then rises to another weak peak at 868 eV before the L_2 line occurs 17.5 eV above the L_3 excitation. Our results for NiO are consistent with Bonnelle's, except that we do not resolve double maxima at the L_{23} lines.

Copper does not exhibit a white line because the 3d conduction band is filled but some fine structure is observed above the L_3 threshold in Fig. 11. [This spectral region is shown with greater energy resolution (2 eV) as the middle curve in Fig. 15 where the filament heating current and hence the beam energy spread was reduced.] Despite the poorer statistics, a series of three peaks is visible centered at 934.5, 938.5, and 942.5 eV, in agreement with x-ray absorption work of Bonnelle[6] and Kiyono *et al.*[10] Structure above the L_2 edge is complicated by overlap of the L_3 structure but a clear second step is observed in Fig. 11 at 959 eV consistent with Kiyono's data. This fine structure will be discussed in more detail in the next section and must be interpreted in terms of the final-state density derived from band calculations. In CuO electron transfer occurs from the 3d orbitals in Cu

to the oxygen atoms to give some unfilled d states. Hence in a rigid-band model, one expects the Fermi level in CuO to be lowered into the Cu d bands, which are themselves assumed to be unchanged by oxidation. This provides an explanation both for the reappearance of the white lines in CuO (although they are much weaker than in NiO; cf. Figs. 5 and 6) and also for the lowered EELS threshold energy of the L_3 edge in CuO compared to Cu noted above in Table I. However, the rigid-band model is an oversimplification, since it ignores the creation of an insulating band gap in the oxide. Nonetheless, it provides a useful framework for interpreting the Cu-CuO spectra at threshold.

C. White-line widths: Comparison between single-particle calculations and experimental results

Here we compare the measured widths of the L_3 white lines and also their fine structure with the results of a systematic linear augmented plane wave (LAPW) calculation for the 3d transition metals by Müller, Jepsen, and Wilkins.[24] Comparisons to other existing calculations are also made. There is no corresponding theoretical development for the oxides.[60]

Table II summarizes the experimental and theoretical results for the white-line widths. Note the following features. (i) The observed L_3 width, i.e., the full width at half-maximum (FWHM), decreases from 4.9 eV in titanium to 3.2 eV in nickel.

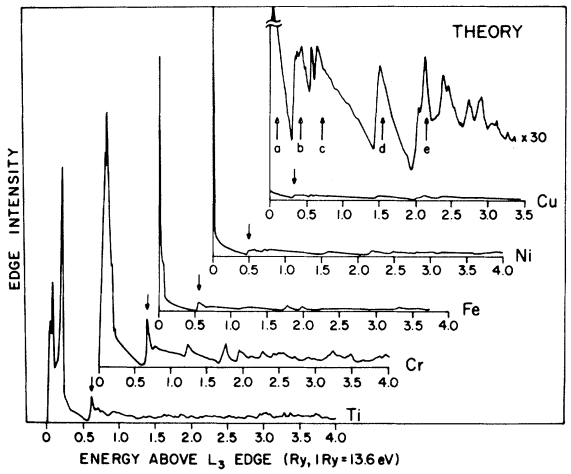

FIG. 13. LAPW calculation for the unbroadened L_3 edges in selected 3d transition metals (Ref. 24).

This decrease is consistent with a model in which the observed width is due to the steadily decreasing width (as Z increases) of the unfilled portion of the 3d band. (ii) The calculated unfilled portion is always smaller than the measured width reflecting the presence of additional broadening mechanisms (discussed below). (iii) The measured white-line width for any oxide is less than that for the corresponding metal (note that Cu has no white line since its 3d band is full).

In Fig. 13 the calculated L_3 absorption spectra[24] are shown for titanium to copper. The principal feature for Ti to Ni is the white line due primarily to transitions from the $2p_{3/2}$ core level into the unfilled portion of the 3d band. The transition into

TABLE II. Intrinsic widths due to core lifetimes for the metal L_3 and L_2 atomic levels from Krause *et al.* (Ref. 33). The measured L_3 white-line widths for the metals and oxides are shown in column 3, and the measured widths corrected for instrumental resolution in column 4. The width of the unfilled portion of the metal 3d band calculated by Müller and Wilkins (Ref. 24) is given in column 5.

Material	Intrinsic width (eV) L_3	L_2	Measured L_3 FWHM	Corrected L_3 FWHM	Calculated empty 3d-band width
Ti	0.22	0.33	4.9±0.3	4.6±0.3	2.9
TiO_2			4.1	4.0	
Cr	0.27	0.47	4.5	4.3	2.6
Cr_2O_3			3.5	3.2	
Fe	0.36	0.65	3.8	3.5	0.7
FeO			2.8	2.4	
Ni	0.48	0.88	3.2	3.0	0.1
NiO			1.9	1.2	
Cu	0.56	1.10			0
CuO			1.8	1.3	

the 4s band (which overlaps the 3d) is considerably weaker due both to the order-of-magnitude smaller transition rate ($2p \rightarrow 4s$, compared to $2p \rightarrow 3d$) and also to the smaller density of 4s band states. The widths of the L_3 white lines in Fig. 13 are estimated from the calculated unfilled 3d-band width given in Table II. We point out also the weak feature some 7–9 eV above the L_3 edge. This feature is due to excitations to orbitals centered on neighboring atoms which are primarily of 4p character but which exhibit some d character at the x-ray excited atom. Finally, in the case of Cu, where there are no unfilled 3d states, the resulting structure is much weaker but, as it turns out, nonetheless observable.

In order to connect the calculated spectra with the observed ones, it is necessary to identify the several broadening mechanisms. These are (i) the instrumental energy resolution, (ii) the finite lifetime of the core hole, and (iii) the finite lifetime of the final excited electron. The instrumental energy resolution arises mainly from the thermal spread of the incident electrons. This resolution function, approximated by a Gaussian about 1.5 eV wide but varying slightly between runs, can be taken into account by subtracting in quadrature the beamwidth from the measured L_3 width (corrected width $=[(\text{measured width})^2-(\text{incident beam width})^2]^{1/2}$). The corrected values are listed in the fourth column of Table II.

Next we consider the intrinsic Lorentzian energy widths due to the finite lifetime of the core hole ($\Delta E \sim \hbar/\tau_{\text{hole}}$). For the L_{23} shell of the 3d transition metals, the most important mechanism for decay is Auger electron emission rather than radiative emission. Table II lists the L_3 intrinsic widths Γ_3 compiled by Krause *et al.*[33] and shows a variation between 0.22 eV for Ti and 0.56 eV for Cu. As discussed by Krause[33] and Fuggle *et al.*[34] there is some uncertainty in the L_2 width (Γ_2). This is because a Coster-Kronig decay channel may be present in the metal even though it is not energetically possible in the case of single atoms. We have assumed that this other decay mechanism does occur and therefore the quantity Γ_2 listed in Table II represents the largest value for the L_2 width. Notice that Γ_2 is never more than 0.5 eV greater than Γ_3 and this difference is considerably smaller than the instrumental resolution.

An additional initial-state broadening mechanism is the possibility of multiplet splitting of the L_{23} levels by interaction with unpaired 3d valence orbitals. This mechanism might effectively broaden the L_3 or L_2 levels and be confused with final-state effects. Kowalczyk *et al.*[61] and Fadley *et al.*[62] have discussed multiplet splitting in terms of XPS spectra. Differences were observed in the shapes of the Mn $2p_{3/2}$ and $2p_{1/2}$ peaks in MnF_2,[61] suggesting the existence of multiplet effects. It is not clear to what extent they are present in the metals but XPS data on Ti and Cu shows $2p_{3/2}$ and $2p_{1/2}$ level widths of only 1 or 2 eV compared with $\sim$4 eV for MnF_2. This indicates that although multiplet splitting occurs in metals, it is much smaller than in MnF_2.

The final mechanism for broadening the theoretically calculated spectra is due to the lifetime of the excited states. Unfortunately at the energies of interest here (up to $\sim$20 eV above onset) the lifetime is very sensitive to the band structure of the unfilled states. Roughly, the final-state width $\Gamma_{FS}(\epsilon)$ increases as $(\epsilon-\epsilon_F)^\alpha$ where α lies between 1 and 2 and $\epsilon-\epsilon_F$ is the energy above the Fermi energy. In copper, Γ_{FS} is approximately 2 eV at an energy 10 eV above the Fermi energy,[63] and Müller *et al.* have used the same dependence for Ni.[64] The above broadening mechanisms have been used to generate theoretical absorption curves which we now compare with the EELS data. For the cases of nickel and copper, we show the comparison between the experimental L_{23} spectra and the LAPW calculation convoluted with a Lorentzian whose width is the sum of the widths from the estimated initial-[65] and final-state lifetimes. Since the instrumental resolution is not included, the theoretical spectra correspond to an experiment with infinite energy resolution, and the corresponding white-line width should be compared to the corrected widths listed in Table II. The calculated spectra were constructed assuming an L_3-to-L_2 intensity ratio of 2:1 based on the initial-state degeneracies.

Figure 14 shows the calculated and measured Ni spectra superimposed with equal L_3 peak intensities. The calculated Ni L_3 white line, with a FWHM of 1.7 eV is significantly narrower than the EELS peak with a FWHM of 3.2 eV even after correction to a FWHM of 3.0 eV for instrumental broadening (see Table II). This difference may be due either to a neglect of multiplet splitting of the 2p core levels or to an underestimation by theory of the unfilled 3d-band width. The weak bump seen above the white line in the calculated curve is a broadened version of the 4p-4d hybridization structure noted previously in the unbroadened edge (Fig. 13). The corresponding experimental bump (Fig. 14) is weaker and broader than the calculated feature, and also lies $\sim$1–0.5 eV lower in energy. The capacity of theory to correctly place this

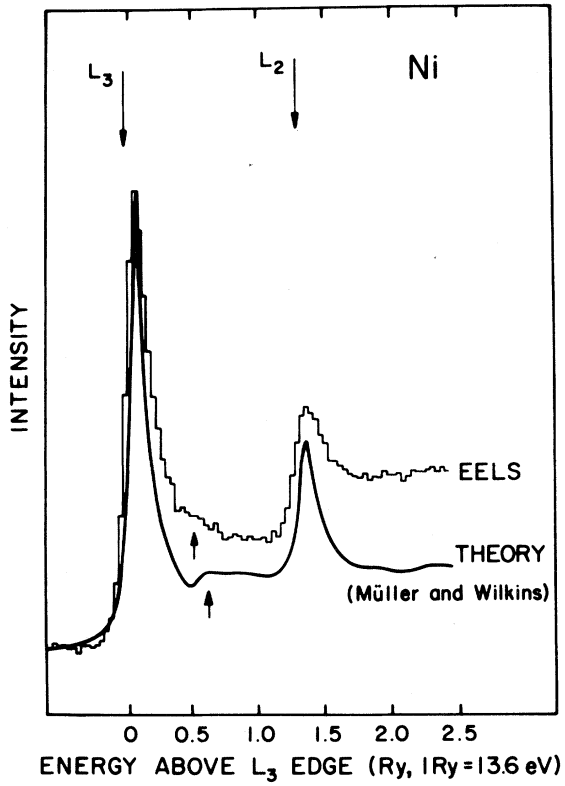

FIG. 14. Calculated and measured Ni L_{23} white-line spectra.

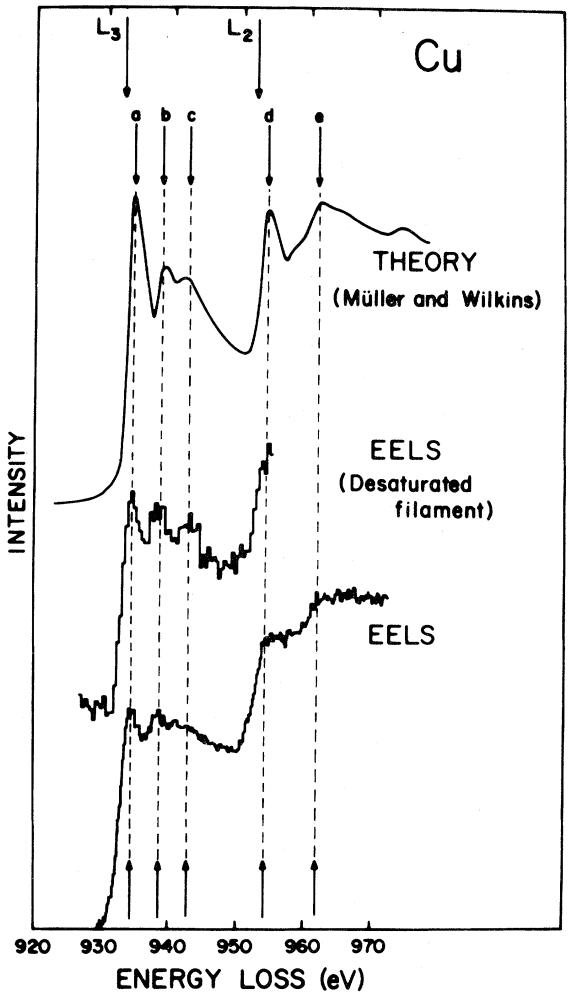

FIG. 15. Calculated and measured Cu L_{23} edge spectra.

feature depends on the construction of the effective potential used in all such calculations. There is the known difficulty that potentials based on the uniform electron gas have in the relative positioning of the d and s bands. Also, there may be a difference between the potential appropriate for calculating excitations compared to the employed potential which is appropriate to ground-state properties.

As expected from the small calculated unfilled d-band widths listed in Table II, the broadened white lines for titanium, chromium, and iron are systematically about 1 eV narrower than the corrected experimental result. The weak $4p$-$4d$ bump is evinced in all the calculated transition-metal L_3 spectra (Ti-Ni). However, inclusion of the L_2 edge at the spin-orbit splitting energy obscures this feature in titanium and chromium, since it coincides with the L_2 white line. Our experimental data shows the expected weak maximum in both nickel (Figs. 10 and 14) and iron (Fig. 9), while we find it absent in chromium and titanium (Figs. 8 and 7) as predicted by the calculation.

The measured and calculated L_{23} spectra for copper are shown in Fig. 15. (The middle EELS edge was obtained at better energy resolution but poorer counting statistics; see III B.) Because the $3d$ band is entirely filled, there is no white line and therefore no broadened white-line tail to wash out the fine structure ($a-e$) appearing in both the calculated and experimental spectra. The calculated peaks may be compared to those appearing in the unbroadened L_3 spectrum in Fig. 13 and their relative positions are in good agreement with experiment. The fine-structure origins are as follows (see both Figs. 13 and 15). A small tail of the $3d$-$4s$ hybridized band remains unoccupied and a peak (a) is therefore visible at threshold. The $4p$-$4d$ bump observed in the transition metals appears in copper as two peaks at 5 eV (b) and 8 eV (c) above threshold, in good agreement with our experimental data. The computed L_3 edge has a peak associated with a $4d$ band, which coincides in energy with the more intense L_2 edge (d). Consequently,

this feature is not resolved in either the calculated or measured L_{23} spectra because of peak overlap. Finally, the calculation shows a broad maximum (e) associated with a 4f band with some d character coinciding with the observed rise in our lower EELS spectrum at 962 eV.

Beside the LAPW study described above there have been several density of states (DOS) calculated by various authors[23,66–70] and in the case of Ni (Refs. 23 and 69) and V (Ref. 66) the 2p absorption edges have also been calculated. These calculations also tend to predict narrower white-line widths than our measured EELS values. Recent calculations for the DOS in paramagnetic chromium[67] give an unoccupied 3d-band width of $\sim$2.5 eV, while our corrected L_3 white line is 4.3$\pm$0.3 eV. The effect of relaxation broadening on the L_3 line shape precludes a direct comparison between these results, but does not appear to explain this difference completely. APW computations for the L_3 absorption edge in vanadium[66] which include both core-level and final-state broadening yield a width of $\sim$4 eV. This result is closer to our experimental values for titanium and chromium, neighboring elements to vanadium in the Periodic Table. Theoretical work by Singh *et al.*[68] on ferromagnetic ion considers minority- and majority-spin states and gives an unoccupied 3d-band width of $\sim$2.2 eV. This compares with our corrected L_3 linewidth of 3.5$\pm$0.3 eV. Calculations for nickel have been carried out by several authors,[23,69,70] and these all show a very narrow spike in the unoccupied d-state density. Determinations of the L_3-edge shape from the DOS all assume a value for the intrinsic $2p_{3/2}$ core-level lifetime. Nagel *et al.*[69] also consider the hot-electron broadening of the final states and find an L_3 white-line width of $\sim$2.4 eV, less than our corrected value of 3.0 eV. Szmulowicz *et al.*[23] suggest that core-level broadening alone is sufficient to obtain reasonable agreement with experiment and these authors calculate an L_3 linewidth of $\sim$2 eV. Anderson *et al.*[70] have carried out a spin-polarized APW computation and find an unoccupied 3d-band width of $\sim$0.3 eV, but no determination was made for the L_{23} absorption edge.

The other DOS calculations for the transition metals also predict the weak maximum observed at several eV energy above the L_3 white line. The computations of Papaconstantopoulos *et al.*[66] for vanadium explicitly show that this feature arises from a 4p-4d hybridized band in agreement with the calculation of Müller *et al.*[24] A DOS for chromium by Laurent *et al.*[67] shows a similar maximum about 8 eV above the sharp 3d peak. Calculations by Szmulowicz *et al.*[23] and Nagel *et al.*[69] for nickel yield a sharp rise in the p and d DOS at $\sim$6.5 eV and 8.5 eV, respectively, above the Fermi level. This feature is visible in both their calculated L_3 spectra, which are broadened by the computed effects of core-level[23,69] and final-state[69] relaxation. Finally, we note that the calculations of Müller *et al.*[24] are consistent with these previous calculations, which is to say they all do a fair job of explaining the experimental results.

D. White-line intensity ratios

On the basis of the $2j+1$ degeneracy of the initial core states and in a one-electron model, we expect the ratio of L_3-to-L_2 intensities to be 2:1. As was mentioned in the Introduction, we find large departures from this value for the L_3 and L_2 white

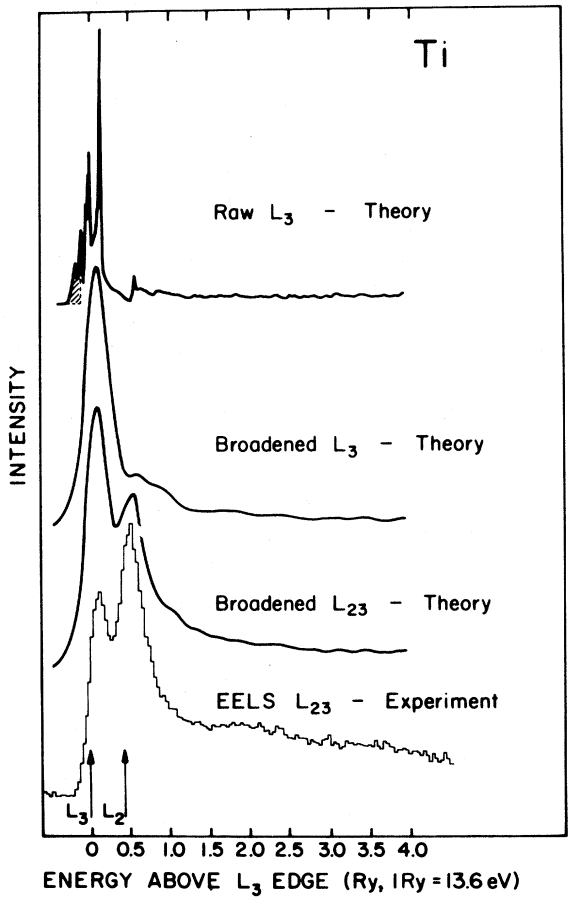

FIG. 16. Ti L_{23} spectrum calculated by assuming a 2:1 L_3-to-L_2 intensity ratio (top three curves). The experimental spectrum (bottom curve) shows an apparent reversal of these peak strengths.

TABLE III. L_3-to-L_2 white-line intensity ratios for the 3*d* transition metals and their oxides including CuO determined by area measurements (column 1) and from the deconvolution (coulmn 2). The result for Cu refers to the ratio of intensities under the L_3 and L_2 steps.

Material	L_3-to-L_2 ratio from areas	L_3-to-L_2 ratio from deconvolution
Ti	0.8	0.7
TiO_2	0.8	0.8
Cr	1.2	1.5
Cr_2O_3	1.7	1.8
Fe	3.0	3.4
FeO	4.1	5.5
Ni	3.1	3.3
NiO	4.0	3.8
Cu	1.7	2.1
CuO	3.5	3.5

lines in the 3*d* transition elements.[5] To illustrate that the value cannot be 2:1, we reproduce at the top of Fig. 16 the calculated unbroadened L_3 edge for titanium (Fig. 13) of Müller *et al.* We then convolute it with a 1.5-eV wide Lorentzian to simulate the various broadening mechanisms discussed in the previous sections (second curve). The broadened L_{23} edge is then constructed assuming an L_3-to-L_2 ratio of 2:1 as was done previously for nickel and copper (third curve). The experimental spectrum (bottom curve) shows an apparent reversal of the relative L_3-to-L_2 peak intensities predicted by this exercise.

intensity ratios, we consider the integrated area under each L_3 and L_2 peak in Figs. 7—10. We recall that the final density of states in these transition metals consists of a narrow sharply peaked 3*d* density of states embedded in a broad free-electron-like band, which is relatively flat as a function of energy. Hence each core edge can be roughly modeled as the sum of a step function arising from transitions to the free-electron-like band and a white line arising from transitions to the 3*d* band. To estimate the white-line ratio we thus extrapolate the step levels back from the tail ends of each of the L_3 and L_2 peaks and measure the areas above the step functions and below the peaks. For Ti where the L_2 and L_3 edges overlap strongly, we use an iterative technique to extrapolate the outlines of the two peaks. This procedure gives L_3-to-L_2 white-line ratios of 0.8, 1.2, 3.0, and 3.1:1 for Ti, Cr, Fe, and Ni, respectively. These are listed in the first column of Table III, together with values for Cu and the metal oxides. In the case of Cu, which does not exhibit white lines, the ratio was taken as the ratio of areas under the L_3 and L_2 steps. A more quantitative estimate of the intensity ratios can be achieved by another method, which is independent of the extrapolation procedure above. First, the background intensity preceding the edge is subtracted off by fitting to a power law E^{-r},[35] where E is the energy loss and $r \sim 3$. The spectrum is then deconvoluted by two δ functions separated by the spin-orbit splitting and whose weights are varied until oscillations in the result are minimized. This deconvolution may be justified by a simple argument. Assume that the measured spectrum $S(E)$ is produced by a core edge line shape $C(E)$, which includes convolution by an instrumental broadening function, evinced with strength g and h at the L_3 and L_2 energies,

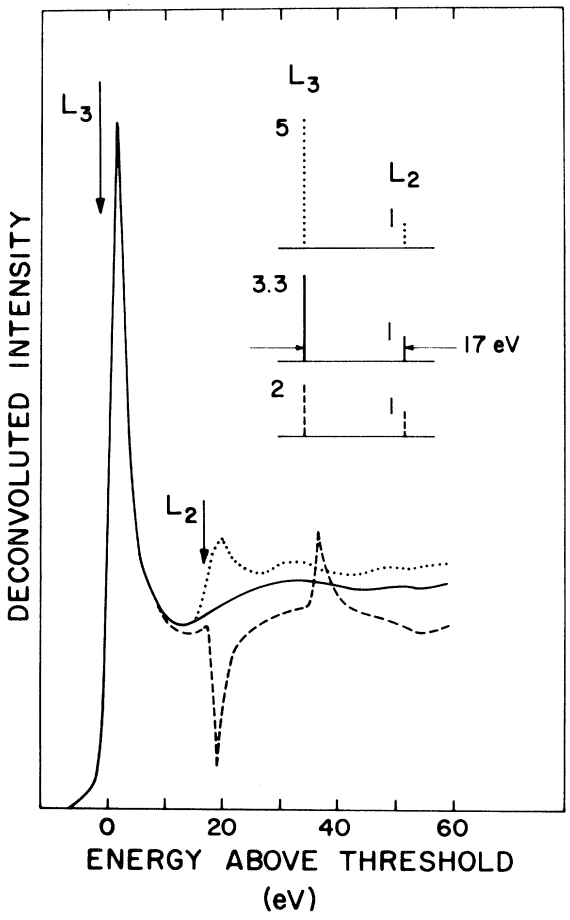

FIG. 17. Ni L_3-edge shape determined by deconvolution of energy-loss spectrum by a pair of δ functions weighted by 3.3:1 and separated by 17 eV (solid curve). Deviations from this ratio leave residual peaks (dotted curve, $g/h = 5{:}1$) or dips (dashed curve, $g/h = 2{:}1$) at the L_2 energy.

respectively. Then

$$S(E)=\int C(E')[g\delta(E-E(L_3)-E') +h\delta(E-E(L_2)-E')]dE' . \quad (6)$$

Making use of the convolution theorem we transform to recover the single core edge line shape by

$$C(E)=F^{-1}\left[\frac{F(S(E))}{F(g\delta(E-E(L_3))+h\delta(E-E(L_2)))}\right], \quad (7)$$

where F denotes a Fourier transform and F^{-1} its inverse. Equation (7) gives a rigorously correct way of removing the L_2 core edge from the tail of the L_3 edge, providing the two peaks possess identical line shapes, and hence allows us to measure g/h despite peak overlap. Incorrect δ-function ratios cause residual peaks or dips at the L_2 energy as illustrated in Fig. 17 for Ni where a value of 3:3:1 is found. Values listed for the other metals and oxides in the second column of Table III agree well with the area measurements above and are accurate to within ±10%. Results show that both Ti and Cr which are on the left side of the transition row exhibit less than the statistical ratio, while iron and nickel together with CuO on the right side exhibit ratios greater than 2:1. The jump ratio for Cu, also estimated using the deconvolution procedure, agrees closely with the statistical value. Hence we deduce that the nonstatistical result in the other elements and oxides is associated with the white lines. Table III shows that the L_3-to-L_2 white-line ratios in the oxides are systematically higher than in the corresponding metals. The greatest difference occurs in Fe where the ratio in the oxide is about 50% larger than that in the metal.

Our observed anomalous L_3-to-L_2 white-line ratios in the 3d transition elements may be contrasted with values obtained for the 4d and 5d transition metals[14] and for the lanthanides,[71] which all show L_3-to-L_2 ratios close to the statistical value of 2:1. We note that departure from a statistical ratio has been reported for Pt (Ref. 59) but this was attributed to spin-orbit splitting in the 5d band giving partly vacant $d_{5/2}$ but filled $d_{3/2}$ states. The selection rules on j forbid $2p_{1/2}\rightarrow d_{5/2}$ transitions so the L_2 white line is absent. For the 3d transition metals, however, the spin-orbit splitting is too small for such an effect to occur.

Our spectrum for Ti agrees with the EELS data of Trebbia[4] recorded at about 3 eV resolution. This author suggests that the observed reversal of L_3 and L_2 intensities is only apparent and is caused by the natural linewidth being comparable with the spin-orbit splitting. However, our data for Ti and TiO_2 in Fig. 7 recorded at ~1 eV resolution indicates a definite anomaly. Our Ni data are consistent with XAS measurements of Bonnelle,[6] who explains an observed L_3-to-L_2 peak jump ratio of 4:1 in terms of an increased L_2 level width. A previous one-electron band calculation for Ni (Ref. 23) also invokes a greater L_2 width to obtain agreement with experiment. As described in the preceding section this effect arises in the 3d transition metals because of the Coster-Kronig decay mechanism for the L_2 hole. However, the most recent data[33,34] show that although this difference is greatest in Fe and Ni and L_2 width exceeds the L_3 by at most 0.5 eV. Taking into account our instrumental resolution, we estimate the total effect on the L_3-to-L_2 integrated intensity ratio as $<10\%$, and this is unable to explain adequately our measured values.

There are a number of other factors which are worth discussing in trying to find a possible explanation for the anomalous white-line ratios. First, we consider measurements of branching ratios in XPS spectra. Significant departures from the statistical result have been found for the $2p_{3/2}$-to-$2p_{1/2}$ (Ref. 72) and the $2d_{5/2}$-to-$2d_{3/2}$ (Ref. 73) branching ratios in a number of elements. This work has mainly been concerned with outer shells, e.g., 4d excitation in Cd and 5d excitations in Hg.[73] The deviation from the statistical value has been explained by two effects: slight differences in the initial-state wave function for $j=l+\frac{1}{2}$ and $j=l-\frac{1}{2}$, and the difference in kinetic energies of the outgoing electron for a particular incident photon energy.[74] In the case of 2p excitation in the 3d transition metals, the difference between the initial-state $2p_{3/2}$ and $2p_{1/2}$ wave functions is very small as is evident from tabulated relativistic data.[75] The second effect does not apply to x-ray absorption or electron-energy-loss experiments because the final-state electron energy is the same for both the L_3 and L_2 excitations. In the XPS experiment, however, the incident photon energy is fixed and the excited electron kinetic energies differ by the spin-orbit splitting. The L_3 and L_2 XPS peaks therefore correspond to different energies above ionization threshold, and it is not surprising that the ratio of cross sections for removing $p_{3/2}$ and $p_{1/2}$ electrons departs from 2:1.

Next we consider the effect of multiplet structure which arises when upon ionization, the angular momenta of the resulting partially filled core

shell couple with the angular momenta of various states of the atom before ionization. Gupta and Sen[76] have calculated the $2p$ multiplet structure for $3d$ transition-metal ions with the configuration p^5d^n ($n=1,\ldots,9$) and the spectra show considerable structure. Two main maxima are still visible at the $p_{3/2}$ and $p_{1/2}$ energies and there appears to be a decrease in the integrated $p_{3/2}$-to-$p_{1/2}$ ratio with increasing ionic charge for Ti and Cr. This is an opposite trend to the one observed in the energy-loss spectra (Table III) which show increased ratios for the oxides over the metals. The XPS data of Kowalczyk *et al.*[61] indicates that the integrated $p_{3/2}$-to-$p_{1/2}$ ratio is near 2:1 across the entire period, suggesting that initial-state multiplet splitting cannot account for the observed variation in the EELS spectra. Nevertheless, their spectra for Fe and Ni shows a $2p_{1/2}$ peak broader than the $2p_{3/2}$ peak and also a subsidiary shoulder on the $2p_{1/2}$ peak not present on the $2p_{3/2}$ peak. This is consistent with our measured L_{23} spectrum for Fe and Ni in Figs. 9 and 10, and suggests that differences in shape between the L_2 and L_3 edges may be due to multiplet effects. However, this does not seem to account for the departure from statistical integrated intensity behavior. Kowalczyk's data[61] were recorded with an incident photon energy much greater than the threshold energy so that final-state effects are unimportant. As far as we know, no XPS spectra have been recorded for the $3d$ transition elements at photon energies just above the $2p$ threshold. Such data might be expected to show a L_3-to-L_2 ratio anomaly similar to ours.[77] At these energies a few eV above threshold the ejected photoelectron stays in the vicinity of the excited atom until the system can relax, so that many-electron effects could be present.

Citrin *et al.*[78] have discussed the anomalous L_3-to-L_2 ratio of $\sim$3:1 in Na in terms of $2p$-$3s$ spin-orbit exchange. In the presence of spin-orbit interaction, the LS coupling limit and its symmetries for the electron hole system are destroyed. Since only singlet components (spin-down core hole) are affected by exchange, intensity branching ratios predicted on the basis of spin-orbit splitting alone can be altered significantly. As described by Onodera[79] and Kotani *et al.*[80] the deviation from the 2:1 statistical value expected on the basis of j-j coupling depends on the ratio of the singlet-triplet exchange splitting Δ to the spin-orbit splitting λ. As $\Delta/\lambda\rightarrow\infty$, the L_3-to-L_2 ratio tends to zero. However, for a metal such as Na, the exchange interaction can be screened, hence reducing Δ/λ and mixing the states. For Na both the exchange and spin-orbit splitting are about 0.2 eV compared with a spin-orbit splitting of $\sim$6 eV in Ti. Also the exchange interaction Δ is expected to be much smaller in Ti than in Na because of less overlap of the conduction states with the initial $2p$ wave function. It would therefore be surprising if this same mechanism could explain our anomalous ratios in the transition metals.

We should finally mention that anomalous L_3-to-L_2 ratios have been observed in some nonmetals. Zimkina *et al.*[81] found a sulfur L_3-to-L_2 ratio of 0.8:1 in SF_6 gas using x-ray absorption spectroscopy. This has been discussed by Nielsen *et al.*[82] in terms of an exchange interaction similar to that mentioned above. Hitchcock *et al.*[83] have also observed an apparently anomalous ratio in the $2p_{3/2}\rightarrow\sigma^*$ and $2p_{1/2}\rightarrow\sigma^*$ transitions at threshold in the Cl L_{23} edge of the chloromethanes. However, it was not possible for these authors to attribute this ambiguously to an anomalous L_3-to-L_2 ratio since another transition could underly the L_2 peak. Thus possible departures from the statistical ratio have been observed in the l_{23} edges of elements quite close to Ti in the Periodic Table. It seems possible in conclusion that some form of exchange interaction might be responsible for a breakdown of the j-j coupling picture in the $3d$ transition period.

E. Extended fine structure

We now consider the modulations in the fine structure extending several hundred eV above the L_{23} edges.[84] This is seen most clearly in our data for Cr where the counting statistics are favorable and no edges interfere with the structure above the L_{23} threshold. The modulations which correspond to EXAFS in photon absorption are determined by final-state interference effects between the outgoing ejected electron wave from the ionized atom and waves backscattered by the surrounding atoms.[85–87] The oscillatory part of the fine structure is given by

$$\chi(k)=\sum_j \frac{N_j}{r_j^2}A_j(k)\sin[2kr_j+\phi_j(k)]\ , \tag{8}$$

where k is the ejected electron wave vector, which is related to the edge energy E_0 and the energy loss E by

$$\hbar^2k^2=E-E_0\ . \tag{9}$$

$A_j(k)$ in Eq. (8) includes the backscattering amplitude factor, as well as the temperature and electron

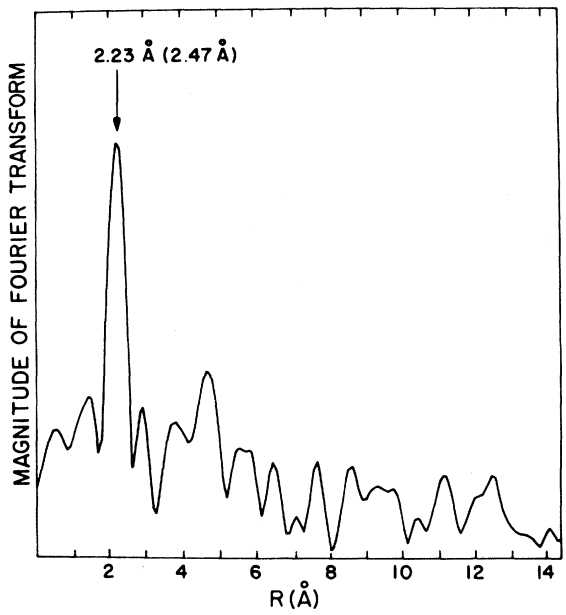

FIG. 18. Calculated radial distribution function in Cr showing nearest-neighbor distance.

range factors; $\phi_j(k)$ is a wave-vector-dependent phase shift due to the central and backscattering atom potentials. Data reduction to obtain the radial distribution function normally would proceed as follows. First, the background after the edge is carefully removed by fitting the intensity to a low-order polynomial, usually a cubic. Second, the resulting EXAFS modulations are replotted on a wave number scale according to Eq. (9). Third, the backscattering amplitude function contained in $A_j(k)$ is taken into account by multiplying the EXAFS by k^2,[88] the appropriate form for atomic numbers near Cr. The intensity modulations are then truncated at $k_{\min}$ and $k_{\max}$. The lower limit is chosen to be ~ 2 Å^{-1} ($\equiv 15$ eV) below which the data is not useful since solid-state effects are dominant. Here the range of the ejected electron is large causing the band structure of the solid to influence the spectrum. The upper limit is set by the energy at which noise begins to dominate or where another edge occurs. Finally, the magnitude of the Fourier transform of the data gives the radial distribution function provided the phase shift $\phi_j(k)$ is taken into account.

In the case of Cr and the other 3d transition metals, analysis is complicated by the overlap of the three L edges, whereas for the higher Z elements these excitations are sufficiently separated in energy for this not to be a problem. For Cr the spin-orbit splitting of 9 eV is small compared with the spacing of extended fine-structure maxima well above threshold. It is therefore reasonable as a first approximation to neglect the L_2 edge. More serious interference arises from the L_1 ($2s \rightarrow p$) excitation at 696 eV. As seen in Fig. 4 there is no sharp edge at this energy, partly because of the comparatively large intrinsic width of the 2s core hole. Denley *et al.*[11] in x-ray absorption work on Ti fitted a cubic polynomial through the broad L_1 peak. Instead we multiply by a step function at this energy so that fits to the background before and after the L_1 edge are continuous. When this background subtraction procedure was used and the oscillations were scaled by k^2, the data was Fourier transformed to give the radial distribution function. The k range was truncated at 2 and 10 Å^{-1}. A strong peak at a distance of 2.23 Å is seen in resulting radial distribution function in Fig. 18. We adopt the calculated phase shift of Teo *et al.*[88] and take only the part linear in k. In fact, Eq. (8) shows that we should add on half the linear part of $\phi_j(k)$ which is ~ 0.24 Å. An upward shift in the radial distribution function by this amount gives 2.47 ± 0.04 Å for the nearest-neighbor distance,

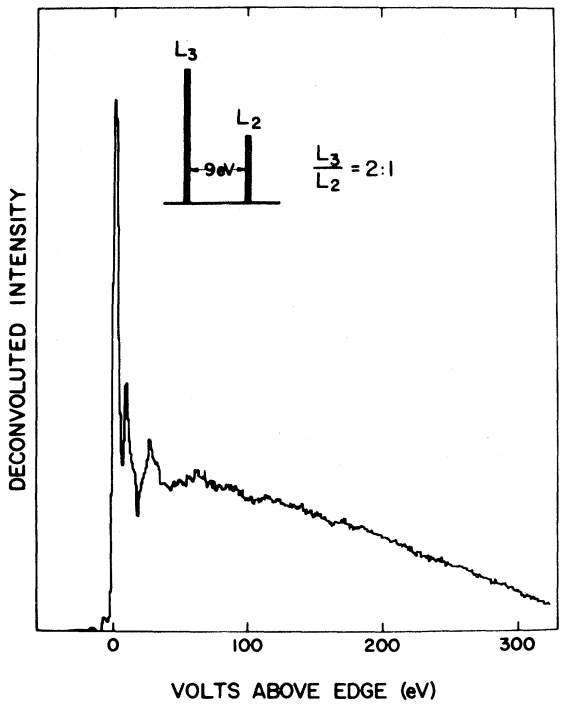

FIG. 19. Results of deconvolution of experimental L_{23} spectrum in chromium by a pair of δ functions spaced 9 eV apart and weighted 2:1. The L_1 intensity was removed first.

agreeing closely with the known radius of the first coordination shell at 2.50 Å in the bcc lattice of chromiun.

It is seen that the second coordination shell is not evident in Fig. 18 even though the resolution should be adequate. This discrepancy may be related to our neglect of the L_{23} spin-orbit splitting. We have therefore attempted to carry the analysis further by separating the L_3 and L_2 contributions to the EXAFS. This was done by a deconvolution in the same way as for determining the L_3-to-L_2 white-line intensity ratios above, except that a 2:1 weight of the δ functions was chosen in order to match the statistical intensity ratio observed in the XPS data.[54] This choice is justified because far above threshold, the EELS excited electron has a wave function closely resembling the free-particle plane-wave state of the ionized electron detected in XPS. The result of the deconvolution is shown in Fig. 19 where the L_2 white line has almost been removed, although a small residual peak still remains. As described earlier, a δ-function ratio of 1.5:1 is required to remove the L_2 line completely. Apart from these differences within the first 10 eV or so above threshold, there are also differences compared to the raw data at higher energies. After the phase shift is added, the computed radial distribution in Fig. 20 now contains a second peak at 3.0 Å consistent with the known second coordination shell at 2.9 Å. Both peaks in the radial distribution function are insensitive to the exact choice of $k_{\min}$ and $k_{\max}$ used to transform the data. A third peak in Fig. 20 at about 4.7 Å (after the phase shift is applied) contains contributions from higher-order coordination shells which are not resolved due to our limited counting statistics. From this analysis, we conclude that it is possible to interpret the extended fine structure above the L_{23} edges in the 3*d* transition elements, provided care is taken to separate contributions from all three *L*-shell excitations. We have also observed EXAFS in the L_{23} edges of transition elements other than Cr (Figs. 3 and 5) but interference from other edges (e.g., oxygen *K* edge in Ti) and insufficient counting statistics in the case of Ni and Cu have prevented us from carrying out a detailed analysis.

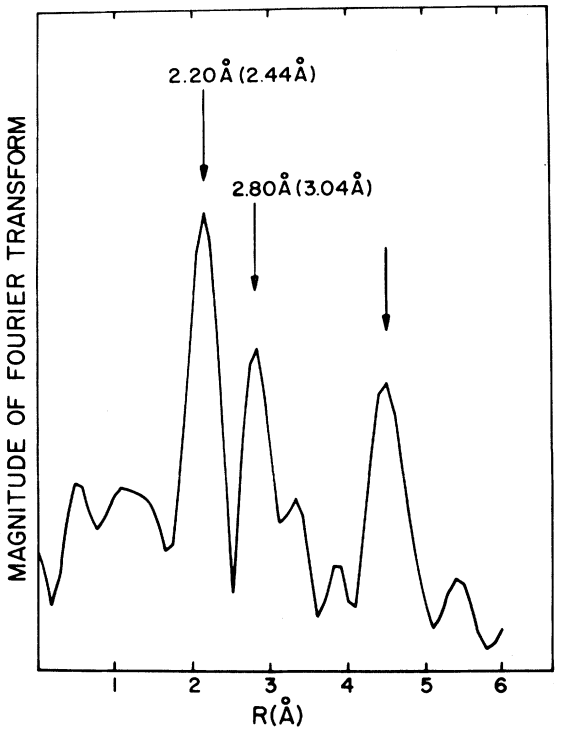

FIG. 20. Radial distribution function obtained from deconvoluted spectrum.

IV. SUMMARY

We have presented data on the 2*p* subshell excitation in half of the 3*d* transition elements and their oxides, the first such study to be carried out using fast electron scattering, and the first systematic study across the row by either EELS or x-ray absorption. The L_{23} edges are dominated by strong "white lines" corresponding to transitions to unoccupied 3*d* states. It is found that the threshold energy shift between metal and oxide is not the same as the XPS chemical shift. Differences are attributed to relaxation effects. We compare our data with the results of a systematic single-particle calculation for the metal L_3 edges by Müller, Jepsen, and Wilkins. The observed and calculated white-line width decreases with increasing atomic number across the period, corresponding to a filling up of the 3*d* band. However, the experimentally measured widths are generally larger than those predicted by theory after broadening by the core-level and final-state lifetimes. Fine structure in the experimental and theoretical L_{23} spectra is in good agreement. An unexpected variation in the L_3-to-L_2 white-line intensity ratio has been observed across the 3*d* transition row. The ratio is less than the statistical result of 2:1 for Ti (0.8:1) and Cr (1.5:1) while it exceeds 2:1 for Fe (3.4:1) and Ni (3.3:1). A similar result holds for the oxides where the ratio appears to be greater than in the corresponding metal. This behavior seems to be associ-

ated with the white lines since Cu with a filled 3d band shows a statistical L_3-to-L_2 jump ratio. The explanation for the observed variation is not clear but it seems possible that there is a breakdown of j-j coupling due to an exchange mechanism. Finally, we have shown the feasibility of carrying out EXAFS-type analysis on the 3d transition metal L_{23} edges using EELS. We have demonstrated a possible procedure for separating out the extended modulations after the two edges. This information about bond lengths complements the near-edge data obtained from the white-line shapes, which contain information about the electronic structure.

ACKNOWLEDGMENTS

We wish to thank Professor J. Silcox, Dr. P. E. Batson, Dr. A. B. Ray, Professor M. Isaacson, Professor V. O. Kostroun, Dr. S. P. Kowalczyk, Dr. J. F. Herbst, and Dr. J. J. Ritsko for helpful discussions. We are especially indebted to Professor J. W. Wilkins and Dr. J. E. Müller for constructively reading the manuscript. Financial support from the National Science Foundation through the Materials Science Center at Cornell University Grant No. DMR 99-24008 and through Grant No. DMR 78-09204 is gratefully acknowledged.

---

*Present address: Biomedical Engineering and Instrumentation Branch, Bldg. 13, Room 3W13, National Institutes of Health, Bethesda, Maryland 20205.

†Present address: Motorola, Inc., 5005 E. McDowell Road, Mail Drop B136, Phoenix, Arizona 85008.

[1]F. C. Brown, Solid State Phys. 29, 1 (1974).

[2]L. V. Azaroff and D. M. Pease, in *X-ray Spectroscopy,* edited by L. V. Azaroff (McGraw-Hill, New York, 1974).

[3]B. Brouseau-Layhaye, C. Colliex, J. Frandon, M. Gasgnier, and P. Trebbia, Phys. Status Solidi B 69, 257 (1975).

[4]P. Trebbia, thesis for Doctor of Science, Université Paris-Sud, France, 1979 (unpublished).

[5]R. D. Leapman and L. A. Grunes, Phys. Rev. Lett. 45, 397 (1980).

[6]C. Bonnelle, Ann. Phys. (Paris) 1, 439 (1966).

[7]I. A. Brytov, S. A. Nemnonov, and S. A. Gribovskii, Fiz. Met. Metalloved. 30, 95 (1970).

[8]D. W. Fischer, J. Appl. Phys. 41, 3561 (1970).

[9]D. W. Fischer, J. Chem. Phys. Solids 32, 2455 (1971).

[10]S. Kiyono, Y. Hayasi, S. Kato, and S. Mochimaru, Jpn. J. Appl. Phys. 17, 212 (1978).

[11]D. Denley, R. S. Williams, P. Perfetti, D. A. Shirley, and J. Stöhr, Phys. Rev. B 19, 1762 (1979).

[12]J. Stöhr, R. Jaeger, J. Feldhaus, S. Brennan, D. Norman, and G. Apai, Appl. Opt. 19, 3911 (1980).

[13]S. M. Heald and E. A. Stern, Phys. Rev. B 16, 5549 (1977).

[14]P. S. P. Wei and F. W. Lytle, Phys. Rev. B 19, 679 (1979).

[15]M. Isaacson, J. Chem. Phys. 56, 1813 (1972).

[16]J. J. Ritsko, P. C. Gibbons, and S. E. Schnatterly, Phys. Rev. Lett. 32, 671 (1974).

[17]G. H. Curtis and J. Silcox, Rev. Sci. Instrum. 42, 630 (1971).

[18]U. Fano and J. W. Cooper, Rev. Mod. Phys. 40, 441 (1968).

[19]H. A. Bethe, Ann. Phys. (Leipzig) 5, 325 (1930).

[20]L. A. Grunes and R. D. Leapman, Phys. Rev. B 22, 3778 (1980).

[21]M. Inokuti, Rev. Mod. Phys. 43, 297 (1971).

[22]E. E. Koch, C. Kunz, and B. Sonntag, Phys. Rep. 29, 153 (1977).

[23]F. Szmulowicz and D. M. Pease, Phys. Rev. B 17, 3341 (1978).

[24]The first report of this work was for the K edges of the 4d transition metals: J. E. Müller, O. Jepsen, O. K. Andersen, and J. W. Wilkins, Phys. Rev. Lett. 40, 720 (1978). Details of the method and of the results can be found in J. E. Müller, O. Jepsen, and J. W. Wilkins, Solid State Commun. (in press), and J. E. Müller, Ph.D. thesis, Cornell University, 1980 (unpublished).

[25]P. E. Batson, Ph.D. thesis, Cornell University, 1976 (unpublished); P. E. Batson, J. Silcox, and R. Vincent, in *Proceedings of the 29th Electron Microscopy Society of America Meeting, Boston,* edited by C. J. Arcenaux (Claitor, Baton Rouge, 1971), p. 30.

[26]B. Watkins and P. L. Fejes, Proceedings of the Cornell Analytical Electron Microscopy Workshop, Cornell Materials Science Center Report No. 3082 (unpublished).

[27]*Powder Diffraction File* (JCPDS—International Centre for Diffraction Data, Swarthmore, PA, 1980).

[28]M. Hansen and K. Anderko, *Constitution of Binary Alloys,* 2nd ed. (McGraw-Hill, New York, 1958).

[29]H. Raether, *Springer Tracts in Modern Physics,* edited by G. Höhler (Springer, Berlin, 1965), Vol. 38, p. 84.

[30]D. M. Pease, Appl. Spectrosc. 30, 405 (1976).

[31]M. Cardona and L. Ley, *Photoemission in Solids I* (Springer, New York, 1978).

[32]L. A. Grunes, in *Proceedings of the 38th Annual Electron Microscopy Society of America,* edited by G. W. Bailey (Claitor, Baton Rouge, 1980), p. 122.

[33]M. O. Krause, J. Phys. Chem. Ref. Data 8, 307 (1979); M. O. Krause and J. H. Oliver, *ibid.* 8, 329 (1979).

[34]J. C. Fuggle and S. F. Alvarado, Phys. Rev. A 22, 1615 (1980).

[35]R. F. Egerton, Philos. Mag. 31, 199 (1975).

[36]L. Ramqvist, K. Hamrin, G. Johansson, A. Fahlman,

and C. Nordling, J. Phys. Chem. Solids 30, 1835 (1969).
[37]G. Bouyssoux, M. Romand, H. D. Polaschegg, and J. T. Calow, J. Electron Spectrosc. 11, 185 (1977).
[38]K. Hirokawa, F. Honda, and M. Oku, J. Electron Spectrosc. 6, 33 (1975).
[39]K. S. Kim, W. E. Boitinger, J. W. Amy, and N. Winograd, J. Electron Spectrosc. 5, 351 (1974).
[40]M. Romand, M. Roubin, and J. P. Deloume, J. Electron Spectrosc. 13, 229 (1978).
[41]The measured absolute energies of the XPS photoelectron depends on the work function of the sample and spectrometer. However, the experiments are carried out in such a way that these effects cancel, since the energies are measured relative to a well-known energy level present in both metal and oxide. For example, a thin layer of gold can be coated on the samples and the Au $4f$ level detected (see, e.g., Ref. 42).
[42]S. B. M. Hagstrom and C. S. Fadley, in *X-ray Spectroscopy,* edited by L. V. Azaroff (McGraw-Hill, New York, 1974).
[43]F. C. Brown, R. F. Bachrach, and M. Skibowski, Phys. Rev. B 13, 2633 (1976).
[44]R. D. Leapman and J. Silcox, Phys. Rev. Lett. 42, 1361 (1979).
[45]E. J. Mele and J. J. Ritsko, Phys. Rev. Lett. 43, 68 (1979).
[46]H. P. Hjalmarson, H. Buttner, and J. D. Dow, Phys. Rev. B 24, 6010 (1981).
[47]L. A. Grunes, R. D. Leapman, C. N. Wilker, R. Hoffmann, and A. B. Kunz, Phys. Rev. B 25, 7157 (1982).
[48]D. C. Cronemeyer, Phys. Rev. 87, 876 (1952).
[49]W. H. Strehlow and E. L. Cook, J. Phys. Chem. Ref. Data 2, 163 (1973), and references therein.
[50]A. Newhaus, Z. Kristallogr. 113, 195 (1960).
[51]L. F. Mattheiss, Phys. Rev. B 5, 306 (1972).
[52]J. A. Iossell, Chem. Phys. 15, 303 (1976).
[53]Other schemes for measuring excitonic shifts yield levels inside the band gap. For example, Gudat *et al.* [Phys. Rev. Lett. 32, 1370 (1974)] have combined the results of photoemission with optical measurements to measure the strength of the electron-hole interaction in LiF present in the Li 1*s* absorption spectrum. They find an excitonic shift to 10 eV below the bottom of the conduction band as compared to a band gap of 13.6 eV. (The dominant excitonic peak is, in fact, only 2.5 eV below the conduction band.) A later and more systematic study by Pantelides [Phys. Rev. B 11, 2391 (1975)] yields similar results for a number of alkali halides.
[54]D. A. Shirley, in *Photoemission in Solids I,* edited by M. Cardona and L. Ley (Springer, New York, 1978).
[55]J. F. Herbst and J. W. Wilkins, Phys. Rev. B 20, 2999 (1979) (see especially Table II); J. W. Wilkins (private communication).
[56]R. L. Martin and D. A. Shirley, in *Electron Spectroscopy: Theory, Techniques and Applications,* edited by C. R. Brundle and A. D. Baker (Academic, New York, 1977), Vol. I.
[57]J. A. Bearden and A. F. Burr, Rev. Mod. Phys. 39, 125 (1967).
[58]D. W. Fischer and W. L. Baun, J. Appl. Phys. 39, 4757 (1968).
[59]M. Brown, R. E. Peierls, and E. A. Stern, Phys. Rev. B 15, 738 (1977).
[60]The available theory does not include the unoccupied bands (e.g., Ref. 51), and the oxide spectra are complicated by core exciton modifications to the line shape (e.g., Ref. 59).
[61]S. P. Kowalczyk, L. Ley, F. R. McFreely, and D. A. Shirley, Phys. Rev. B 11, 1721 (1975); S. P. Kowalczyk (private communication).
[62]C. S. Fadley and D. A. Shirley, Phys. Rev. A 2, 1109 (1970).
[63]D. E. Eastman, J. A. Knapp, and F. J. Himpsel, Phys. Rev. Lett. 41, 825 (1978); see especailly Fig. 3.
[64]J. E. Müller, Ph.D. thesis, Cornell University, 1980 (unpublished).
[65]The initial-state widths for Ni were taken to be 0.94 eV for the L_3 and 1.6 eV for the L_2 [from an XPS study by S. Hufner and G. K. Wertheim, Phys. Lett. 51A, 301 (1975)]. These are somewhat wider than the values compiled by Krause (Ref. 33) listed in Table II. The widths used for Cu were 0.54 eV for the L_3 and 0.98 eV for the L_2 [from an XPS study by L. I. Yin, I. Adler, M. H. Chen, and B. Craseman, Phys. Rev. A 7, 897 (1973)]. These are virtually identical to Krause's values.
[66]P. A. Papaconstantopoulos, D. J. Nagel, and C. Jones-Bjorklund, Int. J. Quant. Chem. Quant. Chem. Symp. 12, 497 (1978).
[67]D. G. Laurent, J. Callaway, J. L. Fry, and N. E. Brener, Phys. Rev. B 23, 4977 (1981).
[68]M. Singh, C. S. Wang, and J. Callaway, Phys. Rev. B 11, 287 (1975).
[69]D. J. Nagel, D. A. Papaconstantopoulos, J. W. McCaffrey, and J. W. Criss, in *Proceedings of the International Symposium on X-ray Spectra and Electronic Structure of Matter,* edited by A. Faessler and C. Wiech (Academic, New York, 1973), p. 51.
[70]J. R. Anderson, D. A. Papaconstantopoulos, L. L. Boyer, and J. E. Schirber, Phys. Rev. B 20, 3172 (1979).
[71]V. O. Kostroun (private communication).
[72]J. A. R. Samson, J. L. Gardner, and A. F. Starace, Phys. Rev. A 12, 1459 (1975).
[73]T. E. H. Walker, J. Berkowitz, J. L. Dehmer, and J. T. Weber, Phys. Rev. Lett. 31, 678 (1973).
[74]K. Codling, J. Electron Spectrosc. 17, 279 (1979).
[75]F. Herman and S. Skillman, *Atomic Structure Calculations* (Prentice-Hall, Englewood Cliffs, 1963).
[76]R. P. Gupta and S. K. Sen, Phys. Rev. B 12, 15 (1975).
[77]B. Sonntag (private communication).
[78]P. H. Citrin, G. W. Wertheim, and M. Schluter, Phys. Rev. B 20, 3067 (1979).
[79]Y. Onodera, J. Phys. Soc. Jpn. 39, 1482 (1975).

[80]A. Kotani and Y. Toyozawa, in *Topics in Current Physics,* edited by C. Kunz (Springer, New York, 1979), Vol. 10.
[81]T. M. Zimikina and W. A. Fomichev, Dok. Akad. Nauk SSSR 169, 1304 (1966) [Sov. Phys. Dokl. 11, 726 (1967)].
[82]U. Nielsen, R. Haensel, and W. H. E. Schwarz, J. Chem. Phys. 61, 3581 (1974).
[83]A. P. Hitchcock and C. E. Brion, J. Electron Spectrosc. 13, 193 (1978).
[84]R. D. Leapman, L. A. Grunes, P. L. Fejes, and J. Silcox, in *EXAFS Spectroscopy: Techniques and Applications,* edited by K. Teo and D. C. Joy (Plenum, New York, 1981).
[85]D. E. Sayers, E. A. Stern, and F. W. Lytle, Phys. Rev. Lett. 27, 1024 (1971).
[86]F. W. Lytle, D. E. Sayers, and E. A Stern, Phys. Rev. B 11, 4825 (1975).
[87]E. A. Stern, D. E. Sayers, and F. W. Lytle, Phys. Rev. B 11, 4836 (1975).
[88]B. Teo and P. A. Lee, J. Am. Chem. Soc. 101, 2815 (1979).

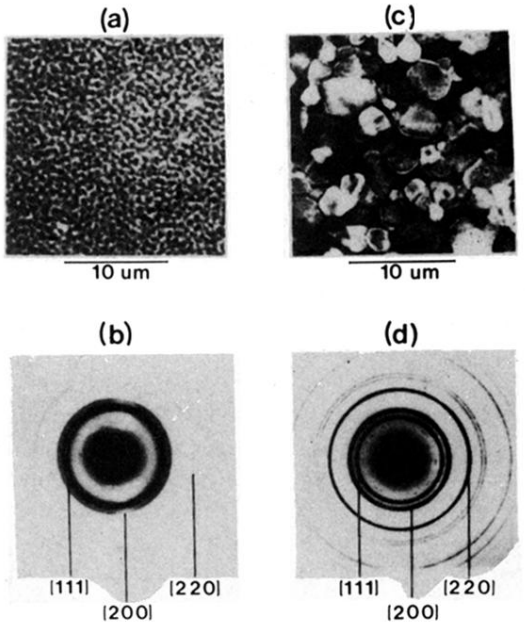

FIG. 1. (a) Electron micrograph of Ni foil showing a grain size of $\sim$20 to 40 nm. (b) Electron diffraction pattern of fcc Ni foil. (c) Electron micrograph of NiO foil showing a grain size of $\sim$2 to 4 μm. (d) Electron diffraction pattern of fcc NiO foil.